Microscopic Approach to Energy Dissipation during Viscoelastic Crack Propagation

NOBUO OHTANI and AKIRA KOBAYASHI, *Institute of Interdisciplinary Research, Faculty of Engineering, University of Tokyo, 4-6-1, Komaba, Meguro-ku, Tokyo, 153, Japan*

Synopsis

The microscopic factors relating to the energy dissipation increase in the viscoelastic dynamic crack propagation such as in PMMA [poly(methyl methacrylate)] were investigated through the observation on the microfracture process ahead of the crack tip up to the microcrack formation. It is found that the energy dissipation remains almost constant in a certain low velocity range but increases sharply in the higher velocity range for the PMMA case. A cleavagelike fracture mode works in the former, and both the cleavagelike and a ductile-fracture mode work in the latter. The increase in energy dissipation is attributed to the secondary cracks which remarkably increase in number depending on the crack velocity. The energy dissipation is proved to be independent of the crack velocity in cases where the crack is propagated by the cleavagelike fracture mode.

INTRODUCTION

The energy dissipation during the viscoelastic dynamic crack propagation sharply depends on the crack velocity.[1] In contrast to the qualitative views expressed in previous works[2–4] with respect to the above dependence, Broberg[5] has recently pointed out that the increase in energy dissipation can be attributed to several factors, i.e., the change of microseparation morphology, winding of the stress field, and so on.

However, the actual fracture process has not yet been interpreted in detail, and the extent of the above-mentioned energy dissipation is unknown. In fact, the energy dissipation in the fracture process occurs in the vicinity of the main crack tip. Thus, in order to clarify the cause, it is necessary to investigate the microfracture process in the vicinity of the main crack tip.

The present paper discusses the correlation between the microscopic factors and the microfracture process at the crack tip corresponding to the increase in energy dissipation in unstable fracture until microcrack formation for the case of PMMA.

TEST SPECIMENS AND EXPERIMENTAL PROCEDURES

The material used was PMMA sheet (Sumipex) produced by Sumitomo Chemical Co., Japan, and was machined into the configuration and dimensions shown in Figure 1. The specimens shown in Figure 1(a) were used for measuring the crack velocity $\dot{C}$ by a velocity gage consisting of silver paint lines at 5-mm intervals on one side of the specimen surface and the dynamic stress intensity factor K_{ID} by the caustic method (described below). The specimens shown in

Journal of Applied Polymer Science, Vol. 29, 1537–1545 (1984)
 CCC 0021-8995/84/051537-09$04.00

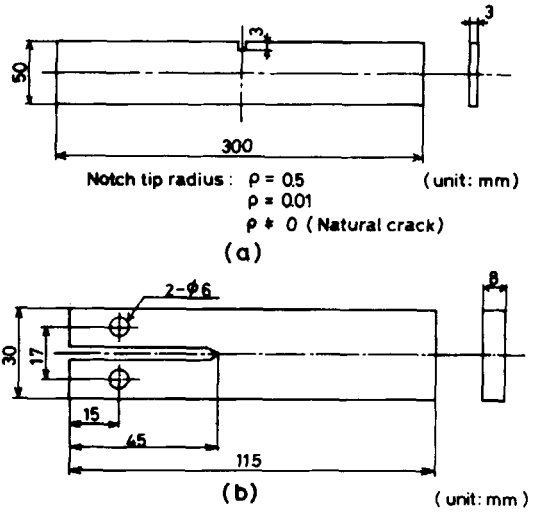

Fig. 1. Configuration and dimensions of a specimen.

Figure 1(b) were employed only to estimate the microfracture process ahead of the crack tip. The former specimens were subjected to tension at a rate of 2 mm/min by a conventional Instron-type tester at room temperature until the unstable fracture in mode I was initiated. The optical arrangement for measuring the dynamic stress intensity factor K_{ID} and the crack length C by the caustic method in combination with a Cranz–Schardin-type high-speed camera is shown in Figure 2. K_{ID} was determined through the following equation[6] by measuring a diameter D_t of a caustic projected on the screen in Figure 2:

$$K_{ID} = \frac{1.671}{Z_0 \cdot t \cdot c_t \cdot \lambda_m^{1.5}} \left(\frac{D_t}{3.17}\right)^{2.5} \tag{1}$$

where z_0 is the distance between the specimen and the screen, t is the thickness of the specimen, c_t ($= 0.551 \times 10^{-10}$ m^2/N) is the stress-optical coefficient, and λ_m [$= z_i/(z_0 + z_i)$] is the magnification (see Fig. 2).

The crack velocity $\dot{C}$ was measured by the ordinary velocity gage method; for further details refer to a previous article.[7] A schematic diagram of the experimental measurement is shown in Figure 3. Figure 4 illustrates the principle of

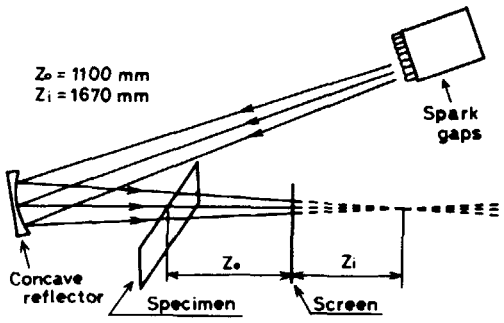

Fig. 2. Optical arrangement for the caustic method.

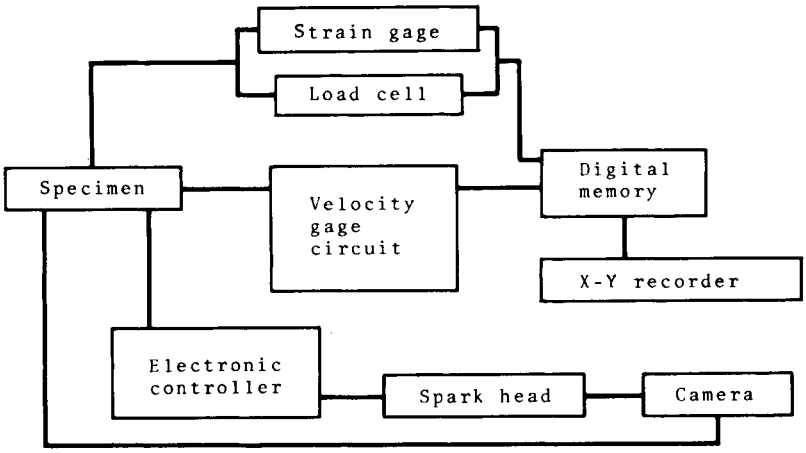

Fig. 3. Schematic diagram for experimental measurements.

the optical system for observing the microfracture process at the crack tip in the stable crack propagation. This technique was applied first by Kambour[8] to study the static morphology of craze material at the crack tip, of which details are shown in Refs. 8–10.

EXPERIMENTAL RESULTS AND DISCUSSION

Energy Dissipation and the Crack Velocity

Figure 5 presents variation of the energy dissipation R as a function of the crack velocity $\dot{C}$ in the dynamic crack propagation range from unstable crack start until the microcrack formation, which is calculated by the following equation[11] using K_{ID} determined through the caustic method:

$$R = \frac{K_{ID}^2}{E} \cdot A(\dot{C}) \qquad \text{(for plane stress)} \tag{2}$$

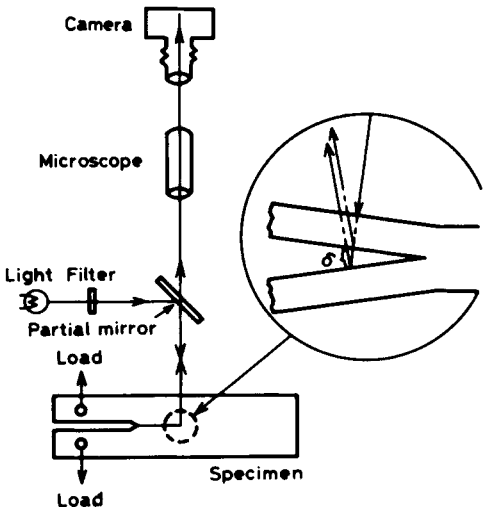

Fig. 4. Illustration of the interference technique.

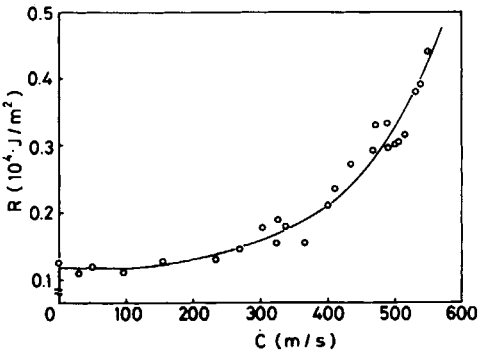

Fig. 5. Relation between the energy dissipation and the crack velocity.

These data were obtained through the specimen shown in Figure 1(a), only. Within a range of $\dot{C} \lesssim 150$ m/s, R increases slightly or remains almost constant from the macroscopic viewpoint. In a range of 150 m/s $\lesssim \dot{C} \lesssim$ 550 m/s, however, R becomes from four to five times larger.

Therefore, it is considered that R is nearly independent of C in a certain low crack velocity range but increases remarkably with increasing $\dot{C}$ in the remaining range.

Energy Dissipation and Microfracture Mechanism

Range Independent of the Crack Velocity. In order to investigate the microfracture mode at the crack tip in the range where R remains almost constant, independent of $\dot{C}$, the fracture surface corresponding to this range was examined through a scanning electron microscope and an optical microscope.

It was found that the morphology of the fracture surface consisted of only irregular lines as shown in Figure 6(a), though it was slightly different, depending on $\dot{C}$. Furthermore, the roughness on the fracture surface obtained by a interference method[12] indicated almost constant value within these crack velocity ranges, as shown in Figure 7 (the tendency of the appearance is approximately

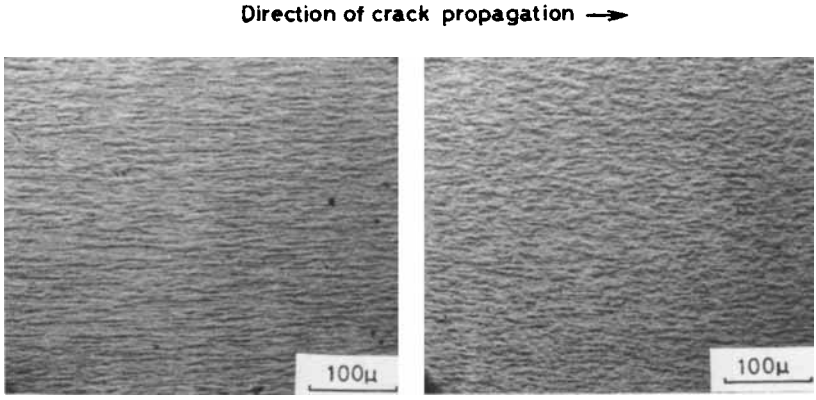

(a) (b)

Fig. 6. Irregular lines.

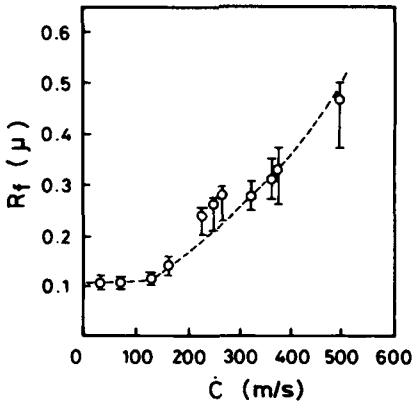

Fig. 7. Variation of the roughness on the fracture surface with the crack velocity.

similar to those in other papers[13,14]). From these results, it is suggested that no change of the fracture mode occurs in this range. Then, the condition for generating the irregular lines was determined in the stable crack propagation under various loading conditions by using the specimens shown in Figure 1(b), and the microfracture process at the crack tip extending under the same loading condition was directly examined by the interference technique illustrated in Figure 4.

Figure 8 shows a micrograph of interference fringes at the crack tip which propagates stably at about 3 mm/s at 28°C, and where irregular lines which are very similar to the appearance of those shown in Figure 6(a) form on the fracture surface as shown in Figure 6(b).

Figure 9 represents a sectional morphology of the crazed layer at the crack tip which is determined through the interference fringes, as shown in Figure 8. In order to depict Figure 9, the following equation[9] was used for calculating the thickness δ of the crazed layer:

$$\delta = \frac{n + 0.5}{2\mu_b} \cdot \lambda \qquad \text{(for bright fringes)}$$
$$\delta = \frac{n}{2\mu_b} \cdot \lambda \qquad \text{(for dark fringes)} \tag{3}$$

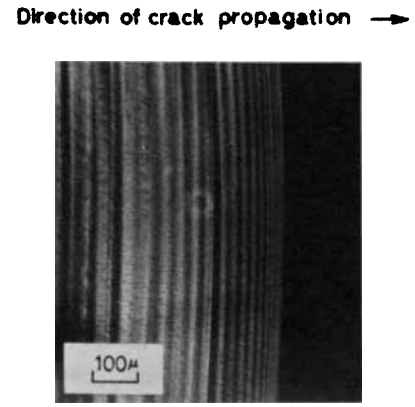

Fig. 8. Interference fringes at the crack tip.

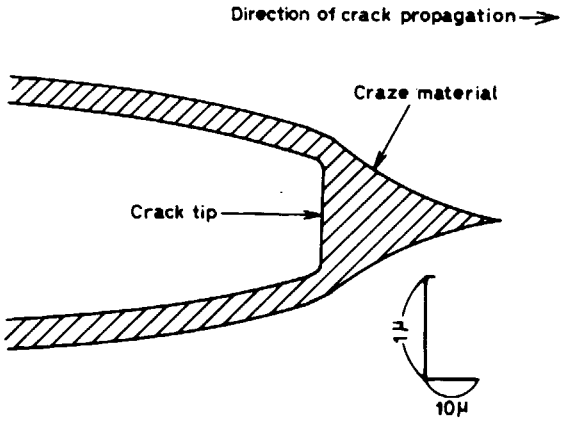

Fig. 9. Sectional morphology of craze material layer at the crack tip.

where n is the fringe number, λ (= 5495 Å) is the wavelength of the incident monochromatic light, and μ_b (= 1.10) is the craze refractive index.

Judging from the similarity of the fractographies between Figure 6(a) (unstable crack) and Figure 6(b) (stable crack) in addition to Figure 9, it was estimated that the fast crack formed the irregular lines as shown in Figure 6(a) should extend by the fracture mode as shown in Figure 9, too. Also, the crack shown in Figure 9 propagates accompanying the same very fine crazed layer at its tip as a plastic zone observed in a cleavage fracture. In the fast crack propagation, the thickness of this crazed layer is estimated to be nearly equal to that shown in Figure 9 by observing the small variation of R_f in Figure 7.

Therefore, it is considered from macroscopic point of view that the fast crack propagation in this range is realized by a cleavagelike fracture mode. In other words, when the crack is extended by the cleavagelike fracture mode, it is supposed that R remains nearly constant.

Range Dependent on the Crack Velocity. Within the range in which R is strongly dependent on $\dot{C}$, it is expected that a change will occur in the fracture

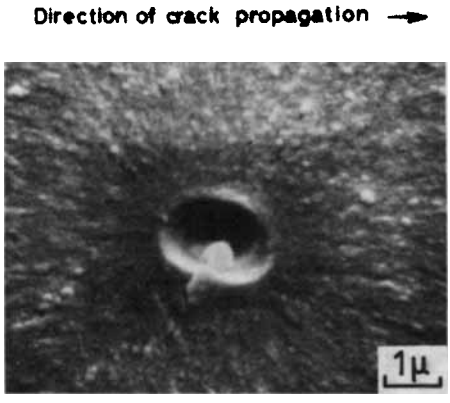

Fig. 10. Secondary crack pit on the fracture surface.

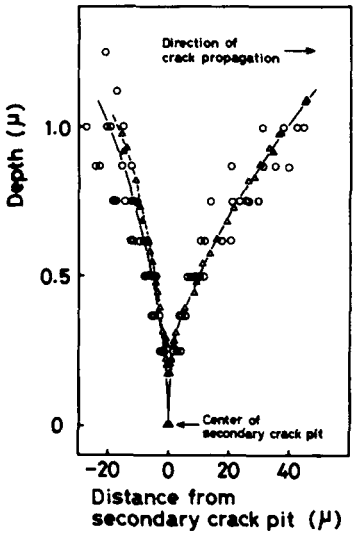

Fig. 11. Morphology of the fracture surface around the secondary crack pit: (O) data obtained through the interference fringes[18] observed around the secondary crack pit; (△) data obtained through the electron microscopic method of Lednicky and Pelzbauer.[19]

mode described above by considering the variation of R_f with $\dot{C}$ as shown in Figure 7. Observation of the fracture surface morphology showed not only the irregular lines, but parabolic marks[13,15] mixed with it which were distributed over this range and increasing[16] depending on $\dot{C}$.

Judging from this change in the fracture surface morphology, it is considered that variation of R in this range is related to the parabolic marks, i.e., the microfracture mechanism forming the secondary crack. It is said that the secondary cracks observed as the parabolic marks are formed ahead of the main crack.[17]

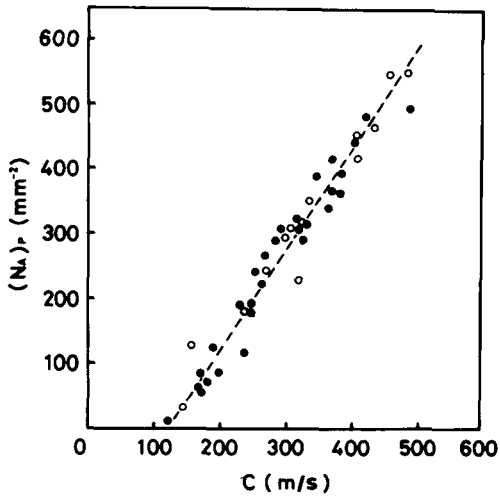

Fig. 12. Relation between the density of the secondary cracks and the crack velocity. Initial crack: (●) natural; (O) notched.

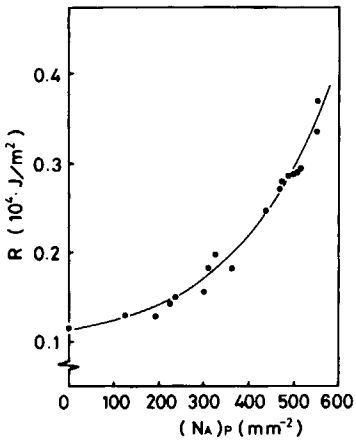

Fig. 13. Correlation between the energy dissipation and the density of the secondary cracks.

Figure 10 shows a microfractography of the secondary crack pit on the fracture surface observed through the scanning electron microscope. This micrograph reveals an inclusion existing at the center of the secondary crack pit as shown in Figure 10. This indicates that the secondary crack is not nucleated by the cavity[13] of the atomic scale in the craze material but caused by the inclusion[15] inherent in the material.

Furthermore, the phenomena are seen in which the microvoid is constantly formed around the inclusion as seen from Figure 10, and the morphology of the fracture surface around the pit always shows a fracture shape like a void coalescence mode (i.e., a ductilelike fracture mode) on both the fracture surfaces in pairs, as shown in Figure 11.

Also, it is considered that the thickness of the crazed layer expands greatly in this velocity range in view of Figure 7. Accordingly, the fracture processes in the secondary crack growth in this case seem to be very similar to those in the common ductile fracture originating from inclusions resulting in coalescence.

From the findings described above, it is suggested that the microfracture mode in this range consists of the cleavagelike fracture mode and the ductilelike fracture mode.

In any case, the fracture appearing in such ductilelike fracture mode will probably require more energy than the cleavagelike fracture mode itself.[20] Therefore, it is anticipated in this case that R will increase with $\dot{C}$. Figure 12 shows the relationship between the density $(N_A)_P$ [= $(N/A)_P$, N, the number of the pits, A, the fracture surface area] of the secondary crack pits, and $\dot{C}$. [These results agree with Carlsson's data,[16] but differ in Cotterell's data[14] in which $(N_A)_P$ does not depend on $\dot{C}$.] This result indicates that the ductilelike fracture mode originates from $C \doteqdot 120$ m/s and increases with $\dot{C}$. Thus, dependence of R on $(N_A)_P$ was rearranged as shown in Figure 13, indicating that R increases remarkably with $(N_A)_P$.

Consequently, it is considered that the remarkable increase in R seen in Figure 6 is attributed to the appreciable increase in the intervention of the initiation and growth of secondary cracks in the fracture process.

CONCLUSION

In order to clarify the dynamic behavior of the energy dissipation and the associated microscopic factors in the dynamic crack propagation up to the microcrack formation in PMMA, the correlation between the microscopic behavior and the energy dissipation was investigated through the observation on the microfracture process ahead of the crack tip.

(1) Energy dissipated during the dynamic crack propagation remains almost constant, independent of crack velocity, in a certain low crack velocity range but increases remarkably in the higher velocity range. The cleavagelike fracture mode works in the former range, whereas both the cleavagelike fracture mode and the ductilelike fracture mode work in the latter range.

(2) The remarkable increase in energy dissipation depending on the crack velocity is attributed to the fact that numbers of secondary cracks increase greatly with increasing crack velocity. That is, the increase in energy dissipation is mainly due to the increase in secondary crack formation.

(3) The energy dissipation is almost independent of the crack velocity when a crack is propagated by the cleavagelike fracture mode.

The authors would like to thank Dr. K. Kurokawa for his helpful discussion and Mr. Y. Fuji and Mr. K. Kodama for their assistance in the present experiments.

References

1. T. L. Paxson and R. A. Lucas, in *Proceedings of an International Conference on Dynamic Crack Propagation*, G. C. Sih, Ed., Noordhoff International, Leyden, 1973, p. 415.
2. B. Cotterell, *Appl. Mater. Res.*, **4**, 227 (1965).
3. J. R. Rice, *Fracture: II*, H. Liebowitz, Ed., Academic, New York, 1968, p. 191.
4. F. Nilsson, Report No. 178, Department of Solid Mechanics, Royal Institute of Technology, Stockholm, 1972.
5. K. B. Broberg, *High Velocity Deformation of Solids*, K. Kawata and J. Shioiri, Eds., Springer-Verlag, Berlin, 1978, p. 182.
6. P. S. Theocaris, *Trans. ASME, Ser. E*, **37**, 409 (1974).
7. A. Kobayashi et al., *J. Appl. Polym. Sci.*, **18**, 1625 (1974).
8. R. P. Kambour, *J. Polym. Sci., A-2*, **4**, 349 (1966).
9. H. R. Brown and I. M. Ward, *Polymer*, **14**, 87 (1973); S. J. Israel et al., *J. Mater. Sci.*, **14**, 2128 (1979).
10. W. Döll et al., *Int. J. Fract.*, **15**, R145 (1979).
11. L. B. Freund, *J. Mech. Phys. Solids*, **20**, 141 (1972); F. Nilsson, *J. Elast.*, **4**, 73 (1974).
12. J. P. Berry, *J. Appl. Phys.*, **33**, 1741 (1962).
13. I. Wolock and S. B. Newman, in *Fracture Processes in Polymeric Solids*, B. Rosen, Ed., Wiley-Interscience, New York, 1964, p. 235.
14. B. Cotterell, *Int. J. Fract. Mech.*, **4**, 209 (1968).
15. E. H. Andrews, in *Fracture in Polymers*, Oliver and Boyd, London, 1968, p. 177.
16. J. Carlsson et al., in *Proceedings of an International Conference on Dynamic Crack Propagation*, G. C. Sih, Ed., Noordhof International, Leyden, 1973, p. 165.
17. C. E. Feltner, Theoretical and Applied Mechanics Report, University of Illinois, 1962, p. 224.
18. R. P. Kambour, *J. Polym. Sci., A*, **3**, 1713 (1965).
19. F. Lednicky and Z. Pelzbauer, *J. Polym. Sci.*, **38**, 375 (1972).
20. H. P. Stüwe, *Eng. Fract. Mech.*, **13**, 231 (1980).

Received June 25, 1983
Accepted November 22, 1983